Novel Nonlinear Droop Control Techniques to Overcome the Load Sharing and Voltage Regulation Issues in DC Microgrid

Prajof Prabhakaran, *Student Member, IEEE*, Yogendra Goyal, and Vivek Agarwal, *Fellow, IEEE*

***Abstract*—In a dc microgrid, good load sharing and voltage regulation are desirable. These are affected by practical factors like sensor calibration errors and cable resistances. To enhance the load-sharing accuracy among the parallel-connected voltage-controlled sources and to improve the dc-bus voltage regulation, three novel nonlinear droop control techniques are proposed for the smart grid scenario. The proposed methods are completely decentralized methods and require only local information (output voltage and output current of the individual converter) for achieving aforementioned merits. Since no communication channel is required, it is easy to implement them. Furthermore, the absence of communication channel improves system reliability and offers plug-and-play features, as only local information is utilized. Also, failure of one converter does not affect the operation of other converters connected to the grid as no information is exchanged between the converters. Effect of sensor calibration errors and cable resistances is minimized by these techniques. Theoretical analysis and experimental results are presented to demonstrate the efficacy of the proposed control methods. Finally, a performance analysis of the three droop control techniques is presented along with their advantages over the conventional methods under different operating conditions.**

***Index Terms*—Control, DC microgrid, droop control, load sharing, stability, voltage regulation.**

I. Introduction

IMPENDING exhaustion of fossil fuels, their rising costs, and concerns about environmental pollution have led to an extensive exploration of renewable energy technology as a part of the smart grid initiative. One of the most effective ways to use renewable energy sources (RES) is to integrate them into the power grid through multiple power conversion stages (dc–dc and dc–ac) [1]. However, the electrical power outputs from most of the RES are inherently dc in nature.[1] Moreover, nowadays, dc loads such as data centers, consumer electronics, variable-frequency drives, and LED lighting systems constitute a significant portion of the energy consuming loads [2]. Therefore, interfacing RES with ac utility grid incurs additional conversion stages (and hence more losses) before any of the loads can use this energy.

Therefore, to efficiently interface the RES and dc loads, dc microgrid systems are proposed as a "smart" solution [3]. Fig. 1(a) illustrates a typical scenario where RES, storage, and loads are connected to an ac microgrid, while Fig. 1(b) illustrates a dc microgrid. From Fig. 1, it may be observed that compared to an ac microgrid, in a dc microgrid, the various loads and sources need only one level of power conversion interface, which improves the efficiency, power transfer capability, ease of control, and stability of the system [3]–[5].

In a dc microgrid, several parallel-connected converters are operated in voltage-controlled mode [6], [7], posing significant challenges like load-sharing accuracy and voltage regulation [8]. Improper load sharing can lead to overloading of converters, thereby causing thermal stress on the switches [7]. To address the abovementioned issue, various control strategies have been proposed in the literature, which are briefly discussed next.

In [8]–[13], droop control schemes based on communication are proposed. Some of the low-bandwidth communication-based methods are: average current sharing [8], voltage sharing [9], and improved secondary control [10]. In [13], a master–slave-type centralized control is proposed. The methods in [8]–[13] restore the dc-bus voltage to the nominal value and enhance the current-sharing accuracy. However, these methods require a communication network for their operation, which increases the system cost and reduces the reliability.

In contrast, the noncommunication-based decentralized droop control schemes [14]–[18] are easier to implement due to the absence of communication infrastructure. They also render plug-n-play feature, higher reliability, and modularity in contrast to the centralized methods. However, most of these methods do not consider the effect of cable resistance and/or sensor gain errors [19]. Furthermore, in these methods, a tradeoff exists between current sharing and voltage regulation.

In [17] and [18], adaptive or nonlinear droop control techniques are proposed, where the tradeoff between voltage regulation and load sharing is minimized, but these methods perform poorly when the converter output current is negative, i.e., when the power transfer is from output side of the converter to its input. Also, the droop gains under light-loading conditions tend to be minuscule resulting in poor load sharing. Clearly, there

Manuscript received November 24, 2016; revised March 6, 2017 and May 6, 2017; accepted June 7, 2017. Date of publication July 4, 2017; date of current version February 1, 2018. Recommended for publication by Associate Editor T.-F. Wu. *(Corresponding author: Prajof Prabhakaran.)*

The authors are with the Department of Electrical Engineering, Indian Institute of Technology Bombay, Mumbai 400076, India (e-mail: prajof@ee.iitb.ac.in; yogendrahnd@gmail.com).

Color versions of one or more of the figures in this paper are available online at http://ieeexplore.ieee.org.

Digital Object Identifier 10.1109/TPEL.2017.2723045

[1]Even if RES such as wind is used which inherently provides an ac, its magnitude and frequency are not compatible with the grid.

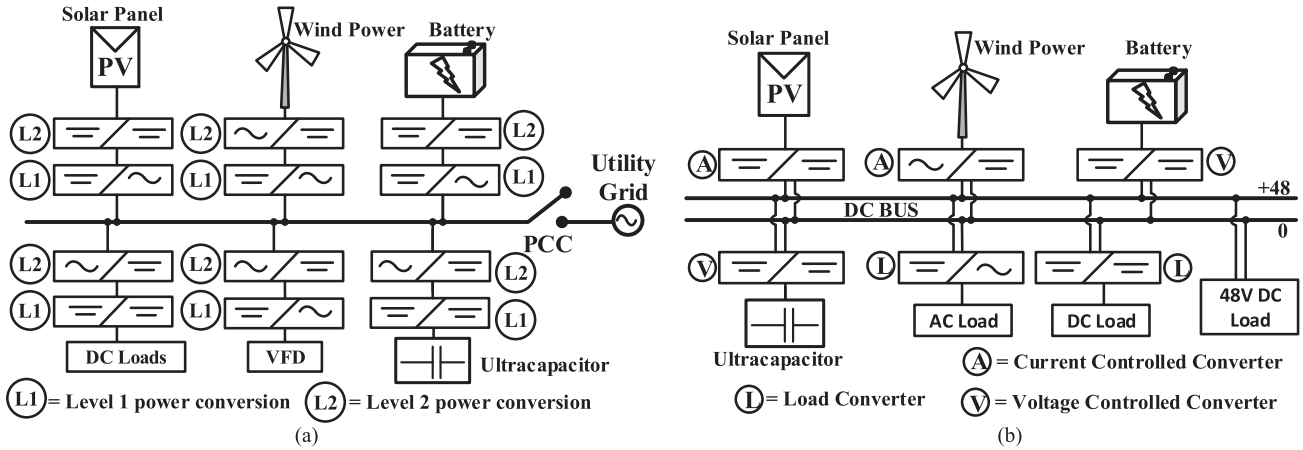

Fig. 1. (a) Typical layout of an AC microgrid; and (b) typical layout of a dc microgrid.

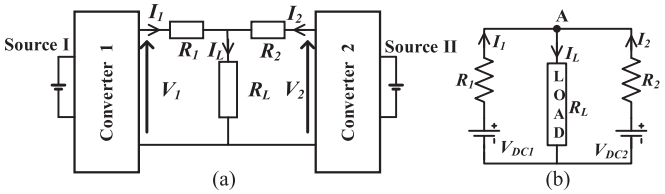

Fig. 2. (a) DC microgrid system with two parallel-connected converters; and (b) equivalent circuit of the system shown in Fig. 2(a).

is a scope for improvement in load-sharing performance by designing proper nonlinear droop curves.

In this paper, three novel nonlinear droop control algorithms are proposed, which address the aforementioned limitations, and also considers the effects of cable resistances and gain errors associated with the voltage sensors. All the proposed schemes adaptively adjust the droop gains based on a few simple algorithms, enhancing the performance in terms of load-sharing accuracy and voltage regulation compared to other existing droop control techniques.

The remaining of this paper is organized as follows: Section II describes the load-sharing issues and their causes. Detailed explanation of the proposed schemes is included in Section III. Section IV presents the stability analysis of the proposed methods. Experimental results are given in Section V. Finally, this paper is concluded in Section VI.

II. Load-Sharing Issues and Analysis of Various Droop Curves

In a dc microgrid, various sources are connected in parallel to share the power in dc grid, as shown in Fig. 1(b). Paralleling of voltage-controlled converters in a dc microgrid leads to load-sharing issues. To analyse these issues, a simple dc microgrid system, consisting of two parallel-connected voltage-mode-controlled converters, is considered as shown in Fig. 2(a). Its equivalent circuit is shown in Fig. 2(b), where $V_{\rm DC1}$ and $V_{\rm DC2}$ are output voltages of the converter 1 and converter 2, respectively. R_1 and R_2 are the cable resistances between converters' output terminals and the load terminal (point A).

Applying Kirchhoff's laws to the circuit of Fig. 2(b), output currents of the two converters can be obtained as follows:

$$I_1 = \frac{R_L(V_1 - V_2) + V_1 R_2}{R_L R_1 + R_L R_2 + R_1 R_2} \quad \text{and}$$
$$I_2 = \frac{R_L(V_2 - V_1) + V_2 R_1}{R_L R_1 + R_L R_2 + R_1 R_2}. \tag{1}$$

In (1), I_1 and I_2 are the output currents of converter 1 and converter 2, respectively. Current-sharing difference between the converters is given by

$$\Delta I = I_1 - I_2 = \frac{2(V_1 - V_2)}{R_1 + R_2 + \frac{R_1 R_2}{R_L}} + \frac{V_1 R_2 - V_2 R_1}{R_L R_1 + R_L R_2 + R_1 R_2}. \tag{2}$$

From (2), it can be observed that if $V_1 = V_2$ and $R_1 = R_2$, then $\Delta I = 0$ or both the converter supply equal currents. However, under practical conditions, there will be a mismatch in voltages V_1 and V_2, due to sensor gain errors. The effective sensed output voltages of converter 1 and converter 2 considering the sensor errors are given by

$$V_1^{\rm eff} = (V_1 \pm K_{v1} V_1); \quad V_2^{\rm eff} = (V_2 \pm K_{v2} V_2) \tag{3}$$

where K_{v1} and K_{v2} are the voltage sensor gain errors of converter 1 and converter 2, respectively.

Furthermore, under most practical conditions, the cable resistances R_1 and R_2 may not be equal. Due to the difference in cable resistance and/or mismatch in terminal voltages, there will be current-sharing differences between the converters (i.e., $I_1 \neq I_2$). The percentage current-sharing error (eI) and voltage deviation (eV) are defined as follows:

$$eI = \left|\frac{\Delta I}{I_1 + I_2}\right| \times 100\%;$$
$$eV = \frac{|V_i^0 - V_i|}{V_i^0} \times 100\% = \frac{\Delta V}{V_i^0} \times 100\%. \tag{4}$$

In (4),V_i, V_i^0, and $I_{\rm i}$ are the actual output voltage, nominal output voltage, and output current of the ith converter,

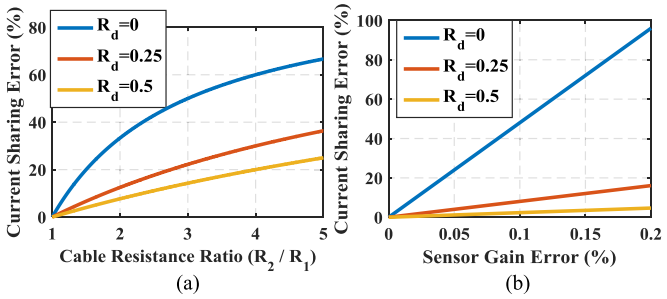

Fig. 3. (a) Effect of cable resistance on current sharing; and (b) effect of sensor gain errors on current sharing.

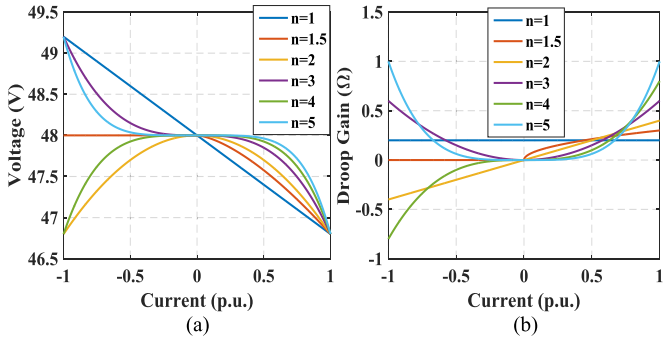

Fig. 4. (a) Droop characteristics (*V* versus *I* curve); and (b) droop gain curves (R_d versus *I* curve).

respectively. ΔV is the maximum allowable voltage dip and $I_{i,\max}$ is the maximum output current of the ith converter.

To improve the current-sharing accuracy, droop control strategy is proposed in [14]. In droop control strategy, a virtual resistance (R_{di}) is added in series with the output terminal of the ith converter. In this case, the output voltage reference for the ith converter is given by

$$V_i^{\text{ref}} = V_i^0 - R_{di} \times I_i\,, \quad \text{where } R_{di} = \frac{\Delta V}{I_{i,\max}}\,. \tag{5}$$

In droop control, the current-sharing difference between the converters is given by

$$\left.\begin{aligned}\Delta I = {} & \frac{2(V_1 - V_2)}{(R_1 + R_{d1}) + (R_2 + R_{d2}) + \frac{(R_1+R_{d1})(R_2+R_{d2})}{R_L}} \\ & + \frac{V_1\,(R_2 + R_{d2}) - V_2\,(R_1 + R_{d1})}{R_L(R_1+R_{d1}) + R_L(R_2+R_{d2}) + (R_1+R_{d1})(R_2+R_{d2})}\end{aligned}\right\}. \tag{6}$$

From (2) and (6), it can be seen that by introducing droop, the current sharing between the converters is improved.

Furthermore, under practical conditions, the nominal voltage in (5) will change due to sensor gain error. The effect of sensor gain error on nominal voltage is given by [20]:

$$V_i^{0\text{eff}} = (V_i^0 \mp K_{vi} V_i) \tag{7}$$

where $V_i^{0\text{eff}}$ is the effective nominal voltage considering the sensor errors, and $\pm K_{vi}$ is the percentage error associated with the output voltage sensor connected to the ith converter's output terminal.

Utilizing (1) to (7), the variation of current-sharing error for different cable resistance ratios and sensor gain errors are plotted in Fig. 3. These plots are obtained for different values of droop gains (R_{di}).

From Fig. 3, it can be seen that high droop gain yields better current sharing. However, high values of droop gain affect the voltage regulation [8]. Hence, in the droop control strategy, good current sharing and improved voltage regulation cannot be achieved simultaneously [8], [17].

From the above analysis, it is evident that in the conventional droop control, a tradeoff needs to be made between current sharing and voltage regulation. However, for a given voltage deviation, the current sharing can be improved further by optimizing the droop trajectory. For a given voltage deviation, there are different ways to draw a droop curve from no-load to full-load operation of the converter. A set of droop curves between two points can be represented by the following general equation [18]:

$$V_i^{\text{ref}} = V_i^0 - k_i \times (I_i)^n,\ n \in R^+;\ \text{where } k_i = \frac{(V_i^{\text{ref}} - V_i^0)}{(I_{i,\max})^n}. \tag{8}$$

From (8), the equivalent droop resistance or droop gain is given by

$$R_{di} = \left|\frac{dV_i^{\text{ref}}}{dI_i}\right| = n \times k_i \times (I_i)^{n-1}. \tag{9}$$

Using (8) and (9), various droop curves and equivalent droop resistances are plotted for different values of "*n*," and are presented in Fig. 4(a) and (b), respectively.

The plots shown in Fig. 4 are obtained considering a nominal voltage (V_i^0) of 48 V, a voltage deviation of 5% (i.e., 46.8 V $\leq V_i^{ref} \leq$ 49.2 V) [21], and maximum output current $(I_{\text{i,max}})$ of 6 A. From Fig. 4, it can be seen that the curves are not symmetric for even and fractional values of "*n*," which leads to asymmetrical performance for the bidirectional operation of converters. Hence, it is suggested to select a droop curve with odd values of "*n*" (i.e., $n = 1, 3, 5, \ldots$). From Fig. 4(b), it can be seen that the droop curve with $n = 3$ offers less droop gain (slope) than the linear droop $(n = 1)$, in the load range of -0.57 p.u. to 0.57 p.u. It is evident from Fig. 4(b) that with an increment in the value of "*n*," the range of converter output current, for which the droop gain stays below the linear curve, increases. This results in worse current sharing compared to linear droop control scheme. Also, it can be seen from Fig. 4(b) that for $n = 3, 5, \ldots$, the value of droop gain is close to zero under light-loading conditions. This drastically deteriorates the current-sharing accuracy under these circumstances. In summary, if the value of "*n*" is small, good current-sharing performance (for same voltage regulation) is achieved for light-load condition, but the current-sharing performance is poor for heavy-load conditions. It is vice versa if the value of "*n*" is large. Hence, there is a scope for improving the current-sharing performance (for same voltage regulation) by hybridizing the positive features of various droop curves shown in Fig. 4. In this paper, an attempt is made to achieve the best tradeoff between

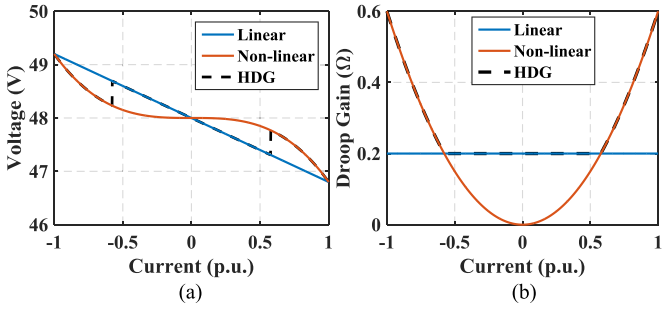

Fig. 5. (a) Droop characteristics for HDG method and (b) Droop gains for HDG method, in comparison with linear and nonlinear droop control methods.

current sharing and voltage regulation by proposing novel nonlinear droop methods by combining the positive features of the various droop curves shown in Fig. 4.

III. Proposed Droop Control Techniques

To overcome the drawbacks of the conventional nonlinear methods discussed above, and to obtain an optimal performance in terms of current sharing and voltage regulation, three novel nonlinear droop control techniques (with odd values of "*n*") are proposed. These techniques are explained in detail in the following sections.

A. High-Droop Gain Method

In Section II, it has been concluded that under light-loading condition, the droop gain value is very low for the droop curve with $n = 3$, leading to a large current-sharing error. Hence, to improve the load sharing even under light-load conditions, a combination of linear and nonlinear schemes is proposed, which utilizes the property of linear $(n = 1)$ and parabolic slope $(n = 3)$ based droop curves. Droop characteristics and droop gains for the HDG method are plotted in Fig. 5(a) and (b), respectively. At each loading condition, the absolute value of the slope of the two curves (see Fig. 5(b)) is compared with each other. The curve with a higher slope is selected to generate the output voltage reference.

The following paragraph explains in detail the logic followed in the implementation of the HDG method.

From (8) and (9), the slope of the linear- and parabolic-based droop curves is obtained by substituting the corresponding value of "*n*" (i.e., $n = 1$ and $n = 3$), and are given as follows:

$$R_{di} = k_i = \frac{(V_i^{\text{ref}} - V_i^0)}{I_{i,\max}} \tag{10}$$

$$R_{pi} = 3 \times \frac{(V_i^{\text{ref}} - V_i^0)\, I_i^2}{(I_{i,\max})^3} = 3k_{pi} I_i^2\,,$$

$$\text{where} \quad k_{pi} = \frac{(V_i^{\text{ref}} - V_i^0)}{(I_{i,\max})^3} \tag{11}$$

where R_{di} and R_{pi} are the droop constants (in Ohms) in the linear and parabolic regions, respectively. In the HDG method, the curve with highest droop gain is selected to compute the voltage reference for the ith converter. That is, when $|R_{di}| > |R_{pi}|$, then the voltage reference is given as

$$V_i^{\text{ref}} = V_i^0 - R_{di} \times I_i \tag{12}$$

and when $|R_{di}| < |R_{pi}|$, then the voltage reference is given by

$$V_i^{\text{ref}} = V_i^0 - k_{pi} \times I_i^3. \tag{13}$$

If there are two converters, say converter p and converter q, with power ratings P_p and P_q, respectively, then the ideal current-sharing ratio between the converters is given by [14]:

$$\frac{I_p}{I_q} = \frac{P_p}{P_q}. \tag{14}$$

For the HDG method, droop coefficients for converters *p* and *q* are designed as follows:

$$\frac{R_{dp}}{R_{dq}} = \frac{P_q}{P_p} \text{ and } \frac{k_{pp}}{k_{pq}} = \left(\frac{P_q}{P_p}\right)^3. \tag{15}$$

From Fig. 5 and from (10) to (15), it can be seen that unlike the parabolic droop method, the HDG method offers a higher droop gain at light-load conditions. Also, unlike the linear droop method, the HDG method offers better current sharing for heavy loading conditions as it offers higher droop gain for a given voltage deviation. However, due to practical factors, the HDG method exhibits poor current sharing near the operating point where linear and nonlinear droop curves intersect. This is because of the following reason: As seen from Fig. 5, ideally, all the converters must shift from linear to parabolic curve when the load current exceeds 0.57 p.u., but due to sensor errors, this shifting does not take place exactly at 0.57 p.u. As a side effect, one converter might operate with linear droop curve, and the other with parabolic droop curve. Hence, under such conditions, the current sharing in the vicinity of 0.57-p.u. load current would be poor.

B. Polynomial Droop Curve (PDC) Method

In the previous section, it was seen that the HDG method yields better results at the light- and heavy-loading conditions. However, its performance is reduced in the vicinity of 0.57-p.u. load current. To overcome this problem, the PDC method is proposed. This method offers relatively high-droop gain under each loading condition and eliminates the discontinuity observed in the HDG method. In the PDC method, least square curve fitting algorithm [22] is used, and a single polynomial curve is obtained to fit the HDG droop gain curve. That is, in the PDC method, only a single PDC is used to realize the droop slope shown in Fig. 5(b).

The general equation of the droop curve in the PDC method is as follows:

$$V_i^{\text{ref}} = V_i^0 - p_5 I_i^5 - p_3 I_i^3 - p_1 I_i. \tag{16}$$

As discussed in Section II, "even" power of the current do not appear in the droop curve (16) as it leads to asymmetric performance. In (16), the values of p_j $(j = 1, 3, \text{and } 5)$ are obtained by the least square curve fitting method [22]. In case of different power ratings of the voltage-controlled converters, the values of p_j $(j = 1, 3, \text{and } 5)$ are obtained as per (15)

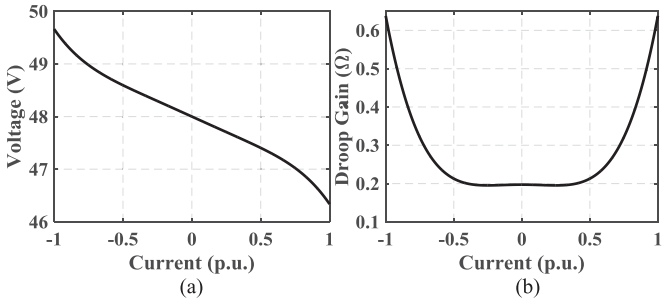

Fig. 6. PDC method: (a) Droop characteristics; and (b) Droop gain curves.

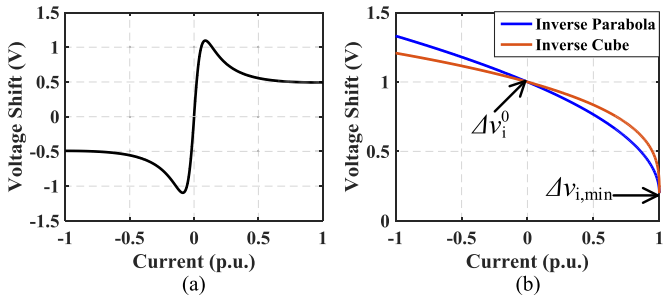

Fig. 7. Δv curve based on: (a) (18); (b) (20), and (21).

to ensure proportional load sharing. Fig. 6(a) and (b) shows the droop characteristics and droop gain curves for the PDC method, respectively.

From Fig. 6(a), it can be seen that the voltage deviation at rated current (1 p.u.) is slightly more than expected 1.2 V. However, it can be seen that for the same voltage deviation, the performance of the PDC method is better than the linear [14] and inverse parabola (IP) [17] methods.

To further improve the load sharing, a higher order PDC can be used to fit the droop gains of multiple droop curves (e.g., $n = 1$, 3, and 5) obtained via HDG strategy. This higher order PDC improves the load sharing, but it deteriorates voltage regulation near the rated loading condition. Nevertheless, the performance would still be better compared to linear [14] and IP [17] droop curves for the same voltage deviation.

C. Polynomial Droop Curve With Voltage Compensation (PDCVC) Method

In the previous section, it was observed that the PDC method provides better current sharing under various loading conditions. However, under heavy-loading conditions, the voltage regulation performance is not as expected. To compensate this, a voltage compensation method is proposed. This new technique of adding a voltage compensation to the PDC is termed as the PDCVC method. In the PDCVC method, the voltage compensation uses only local information, thus preserving the fundamental motive behind the droop control strategy. The generated voltage shift ($\Delta v_{\rm i}$) is added to the output voltage reference of the ith converter. The modified droop equation can be written as follows:

$$V_i^{\rm ref} = \left(V_i^0 - p_5 I_i^5 - p_3 I_i^3 - p_1 I_i\right) + \Delta v_i \qquad (17)$$

where $\Delta v_{\rm i}$ is given as follows:

$$\Delta v_i = \frac{m_1 \times I_i}{m_2 + I_i^2} + \frac{I_i}{|I_i|} \times m_3 \times \sqrt{|I_i|}\,. \qquad (18)$$

In (18), I_i is the actual output current (not in p.u.) of the ith converter. The values of m_1 and m_2 are obtained based on the desired values of $\Delta v_{i,\max}$ and the converter output current corresponding to $\Delta v_{i,\max}$. Here, $|\Delta v_{i,\max}| = 1$ V and $|I_{i,(\Delta v = \Delta v\max)}| = 0.08333$ p.u. (i.e., 0.5 A) are considered. That is, $\frac{d(\Delta v_i)}{dI_i} = 0$ when $I_i = {\rm I}_{i,(\Delta v = \Delta {\rm v}\max)}$. Under such low value of output current (i.e., when $I_i = I_{i,(\Delta v = \Delta v\max)} =$ 0.08333 p.u.), (18) can be approximated as

$$\Delta v_i \approx \frac{m_1 \times I_i}{m_2 + I_i^2}. \qquad (19)$$

From the aforementioned conditions and from (19), $m_1 = 1$ and $m_2 = 0.25$ are obtained. The value of m_3 is obtained such that $d(\Delta v_i)/dI_i \leq 0$ till $I_i = 1$ p.u. (i.e., 6 A). This condition is incorporated to ensure the stability of the system. By using this condition, $m_3 = 0.1333$ is obtained. Fig. 7(a) shows the nature of Δv curve, obtained by varying I_i. The curve shown in Fig. 7(a) is termed as torque based (TB) shift curve as it resembles the torque-slip characteristics of a $3-\phi$ induction motor.

The PDCVC method with the voltage shift function, shown in (18), overcomes the drawback of the PDC method and provides better voltage regulation under high-loading conditions. In the next section, it is proved that the voltage shift function shown in (18) has no side effect on the stability of the system. Also, since there is an inherent droop in the voltage shift (see Fig. 7(a)), it avoids the voltage racing condition. However, for -0.0833 p.u. $\leq I_i \leq 0.0833$ p.u. (light-load condition), the value of Δv_i may be unsymmetrical for different converters due to the sensor gain error. Due to this asymmetry, the load sharing near light-loading conditions is poor. Nevertheless, this poor load sharing is affordable as the current sharing at light load is not critical.

Generally, $\Delta v_{i,\max}$ is selected between 0.8 and 1.2 V (i.e., 1.6% to 2.5% of the nominal voltage of 48 V). This is because if $\Delta v_{i,\max}$ is selected less than 0.8 V (1.6% of $V_{\rm nom}$), then the voltage compensation might not be sufficient to keep the dc-bus voltage in stiff regulation. On the other hand, selecting $\Delta v_{i,\max}$ beyond 1.2 V (2.5% of $V_{\rm nom}$) will cause overcompensation of dc-bus voltage under certain loading conditions. Similarly, $I_{i,(\Delta v = \Delta vi,\max)}$ is selected between 0.05 and 0.25 p.u. of the rated converter output current. This is because, if $I_{i,(\Delta v = \Delta vi,\max)}$ is selected less than 0.05 p.u., then it may lead to extremely poor regulation under light-loading conditions. Furthermore, if $I_{i,(\Delta v = \Delta vi,\max)}$ is selected beyond 0.25 p.u., then there will be poor current sharing for a wide range of load current. Hence, 1.6% of $V_{\rm nom} \leq \Delta v_{i,\max} \leq 2.5\%$ of $V_{\rm nom}$ and 0.05 p.u. $\leq I_{i,(\Delta v = \Delta vi,\max)} \leq$ 0.25 p.u. are the constraints used in designing the coefficients m_1 and m_1 in (18).

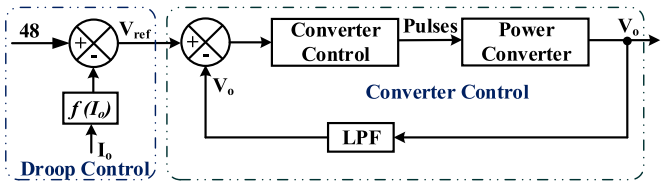

Fig. 8. General droop control structure.

An alternate equation of Δv_i, overcoming the drawback of (18), is given by the following equations:

$$\Delta v_i = \Delta v_{i,\min} + (\Delta v_i^0 - \Delta v_{i,\min}) \times \sqrt{\left(1 - \frac{I_i}{I_{i,\max}}\right)} \tag{20}$$

$$\Delta v_i = \Delta v_{i,\min} + (\Delta {v_i}^o - \Delta v_{i,\min}) \times \sqrt[3]{\left(1 - \frac{I_i}{I_{i,\max}}\right)}. \tag{21}$$

Fig. 7(b) shows the voltage shift curve corresponding to (20) and (21). Since (20) is an IP equation, the shift curve is called IP. Similarly, the curve represented by (21) is termed as inverse cube. It can be seen that the voltage shift equation incorporated using (20) or (21) provides good current-sharing accuracy under all loading conditions compared to the voltage shift equation incorporated using (18). However, from Fig. 7(b), it can be seen that Δv is not symmetric for positive and negative loading conditions. Furthermore, Δv is positive for negative loading conditions. Hence, voltage shift incorporated using (20) or (21) will have poor voltage regulation in the negative current mode.

IV. Stability Analysis for the Proposed Methods

To check if the proposed methods have any side effect on the stability of the system, a detailed stability analysis of the system is carried out with the proposed droop control methods. Eigenvalue approach is followed for this purpose [23].

The generalized control structure of droop control is presented in Fig. 8. From Fig. 8, it can be observed that the output voltage reference of the converter varies with output current. Here, $f(I_{\rm o})$ represents the droop equation, while $V_{\rm o}$ and $I_{\rm o}$ are the converter output voltage and current, respectively. For the ith converter, $f(I_{\rm o})$ can be written as follows:

$$f(I_0) = k_i \times (I_{0,i})^n, n \in R^+; \quad \text{where } k_i = \frac{\Delta v_{i,\max}}{I_{i,\max}^n}. \tag{22}$$

For stability analysis and to investigate the transient behaviour of the system, the dc microgrid model shown in Fig. 2(b) is modified incorporating the cable parameters and a more detailed dc load model as shown in Fig. 9. As dc microgrid is a power electronic intensive power system, most of the loads are connected through dc–dc converters or inverters. In most of these load-interfacing power-electronic converters, the output voltage across the load is tightly regulated. These loads behave as constant power loads (CPL), which have negative impedance characteristics as seen from the input terminals of the power–electronic converter [24]. To make the stability analysis more realistic, a linearized model of CPL is included in Fig. 9 [24].

In Fig. 9, L_1 and L_2 represent the line inductances, R_1 and R_2 are the line resistances, $R_{\rm CIL}$ is the equivalent model of the constant impedance load (CIL), and the combination of $R_{\rm CPL}$ and $I_{\rm CPL}$ is the linearized equivalent model of CPL. The various parameters considered for stability analysis are given in Table I.

To simplify the analysis, the converter dynamics are modeled as a first-order system [23]. The model is simplified in such a way that the properties of converter dynamics are preserved. The simplified model obtained is given as follows:

$$\frac{v_o}{v_{o,\rm ref}} = \frac{1}{\tau s + 1}. \tag{23}$$

In (23), τ is the equivalent time constant of the converter dynamics. Based on the aforementioned assumption, the small-signal model of the system is derived. The details of the derivation are presented in Appendix. For the stability analysis, the output current, the output voltage, and the dc-bus voltage are considered as state variables. The obtained state variable matrix is as follows:

$$x = [v_b \;\; v_1 \;\; v_2 \;\; i_1 \;\; i_2]^{\,T}. \tag{24}$$

In (24), v_1, v_2, i_1, and i_2 are the converter output voltages and currents, respectively. v_b is the dc-bus voltage or voltage across the load terminals. The state-space model incorporating the small-signal analysis for the state variables is given by

$$\dot{x} = Ax \tag{25}$$

where "*A*" is the state matrix.

For the HDG method, two sets of state matrices are obtained based on the values of converter output currents. The state matrix corresponding to droop curve (22) is obtained and presented in Appendix. In the HDG state matrix $(A_{\rm HDG})$, "*n*" is chosen as 1 and 3, based on the converter output current (as explained in the HDG strategy). The values of k_1 and k_2 are obtained as per (8). Fig. 10 shows the locus of eigenvalues (with HDG method) for the system shown in Fig. 8. In Fig. 10, eigenvalues are shown for $n = 1$ and $n = 3$.

In Fig. 10(a), eigenvalues are plotted for increasing CPL and with a fixed value of cable impedance (as per Table I). Here, the CPL is varied from 0 to 200 W. It is observed that the eigenvalues become positive when the penetration of CPL exceeds beyond CIL. This phenomenon has been reported by various researches in the past [24], [25]. Fig. 10(b) shows the locus of eigenvalues for increasing cable inductance (*L*). The cable inductance ranges from 10 to 200 μH, while the total load is kept fixed at 600 W. The locus of eigenvalues, shown in Fig. 10(c), is obtained by plotting the system eigenvalues by varying the cable resistance from 3 to 120 mΩ, at a fixed total load of 600 W.

For PDC and PDCVC methods, the droop coefficients (p_j) shown in (16) and (17) are obtained as per the specifications given in Table I and are as follows:

$$p_1 = 0.1972; \; p_3 = -0.0005845; \; p_5 = 0.00007777. \tag{26}$$

Stability analysis for PDC and PDCVC methods is performed on similar lines as the HDG method. Figs. 11 and 12 show the

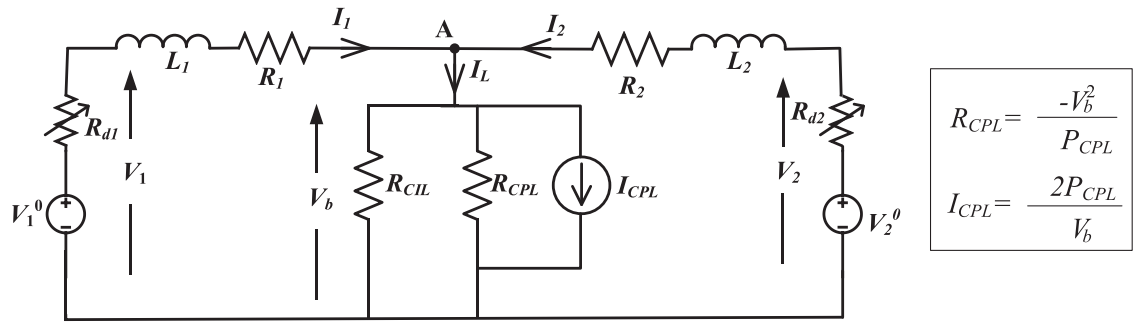

Fig. 9. System model for stability analysis.

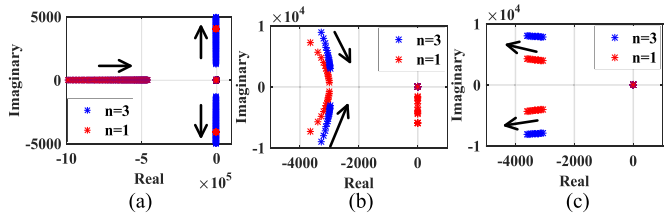

Fig. 10. Locus of eigenvalues for HDG method for (a) increasing load P_{CPL}; (b) increasing cable inductance L; and (c) increasing cable resistance R.

TABLE I
PARAMETERS FOR STABILITY ANALYSIS

V_1^0, V_2^0	R_1, R_2	L_1, L_2	R_{CIL}	P_{CPL}	$\Delta v_{1,\max}$, $\Delta v_{2,\max}$	$I_{1,\max}$, $I_{2,\max}$
48 V	30 mΩ	10 μH	5.76 Ω	200 W	1.2 V	1.2 V

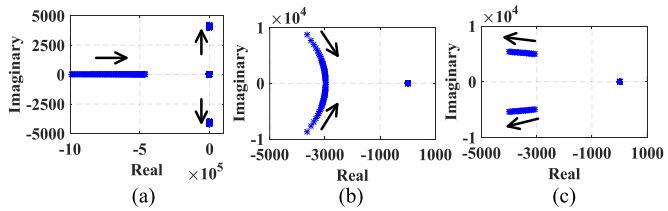

Fig. 11. Locus of eigenvalues for PDC method for (a) increasing load P_{CPL}; (b) increasing cable inductance L; and (c) Increasing cable resistance R.

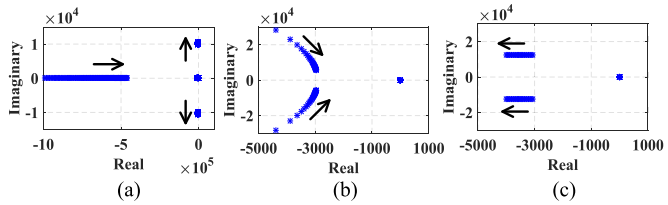

Fig. 12. Locus of eigenvalues for PDCVC method for (a) increasing load P_{CPL}; (b) increasing cable inductance L; and (c) increasing cable resistance R.

locus of system eigenvalues for the PDC and PDCVC methods, respectively.

From Figs. 10–12, it can be seen that the real part of the eigenvalues is negative, indicating that the system is stable for the considered variation of CPL and cable parameters.

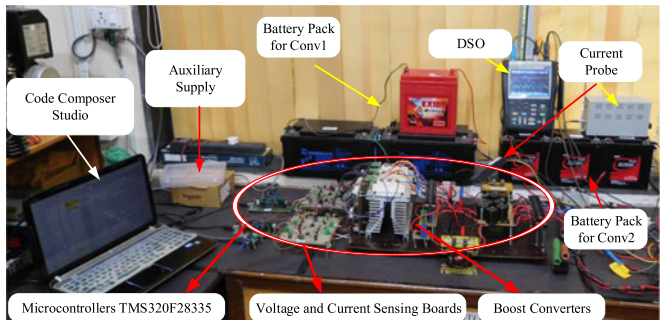

Fig. 13. Photograph of the experimental setup.

TABLE II
CONVERTER PARAMETERS

Parameter	Symbol	Value
Battery parameter	$V_{\mathrm{in},i}$	36 V, 26 AH
Nominal voltage	v_i^0	48 V
Inductance	L_i	250 μH
Inductor ESR	r_{Li}	100 mΩ
Input capacitor	C_i	1000 μF
Output capacitor	C_o	2000 μF
ESR	r_{Ci}	60 mΩ
Power rating	$P_{i,\max}$	300 W each

V. EXPERIMENTAL RESULTS

To validate the performance of the proposed droop control method, a dc microgrid prototype of 1.2 kW is built. The dc microgrid prototype consists of two voltage-controlled converters (300 W each), two current-controlled converters (300 W each), one resistive load, and one dc electronic load. The voltage-controlled converters are battery fed bidirectional boost converters. These converters operate in voltage control mode [26] and regulate their output voltage by incorporating one of the proposed droop control strategies (see Fig. 8). The voltage and current compensators for the same are designed based on the k-factor approach [27]. Fig. 13 shows the photograph of the experimental setup.

The converter and control parameters are listed in Tables II and III, respectively. Lead acid batteries are used as sources for the voltage-controlled converters. The control of the individual converter is carried out using TMS320F28335 DSP microcontroller from Texas Instruments. The performance of

TABLE III
CONTROL PARAMETERS

Parameter	Symbol	Value
Switching frequency	f	30 kHz
LPF cutoff frequency	f_c	7.2 kHz
DC-bus voltage variation	$\Delta V_{i,\max}$	$\pm$1.2 V
Voltage sensor error	k_v	$\pm$0.5%
Cable resistance	R_1	10 mΩ
	R_2	20 mΩ
Maximum output current	$I_{i,\max}$	6 A

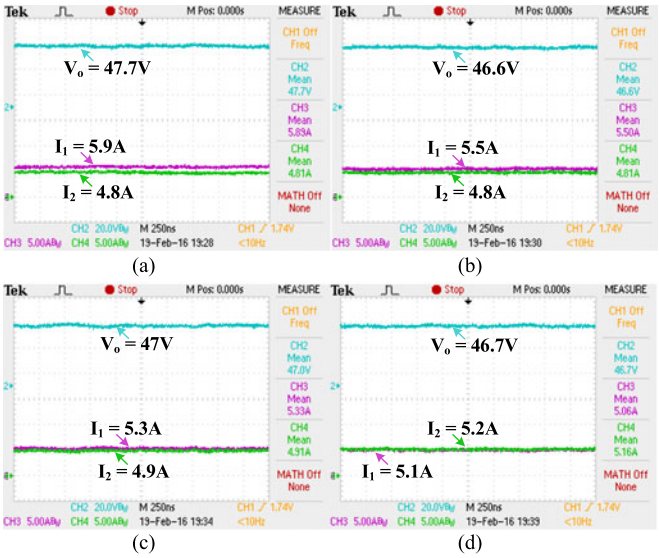

Fig. 14. Converter output currents (5 A/div) and dc-bus voltage (20 V/div) for a load of 500 W, with (a) HDG; (b) PDC; (c) PDCVC IP shift; and (d) PDCVC TB shift method.

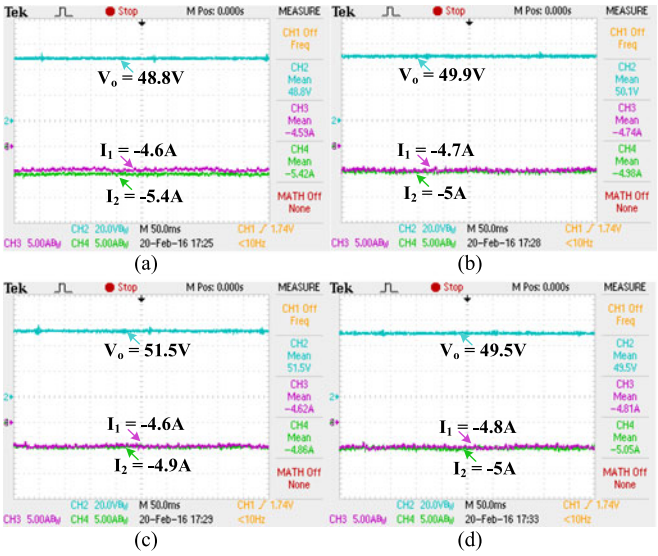

Fig. 15. Converter output currents (5 A/div) and dc-bus voltage (20 V/div) for a load of $-$500 W, with (a) HDG; (b) PDC; (c) PDCVC IP shift; and (d) PDCVC TB shift method.

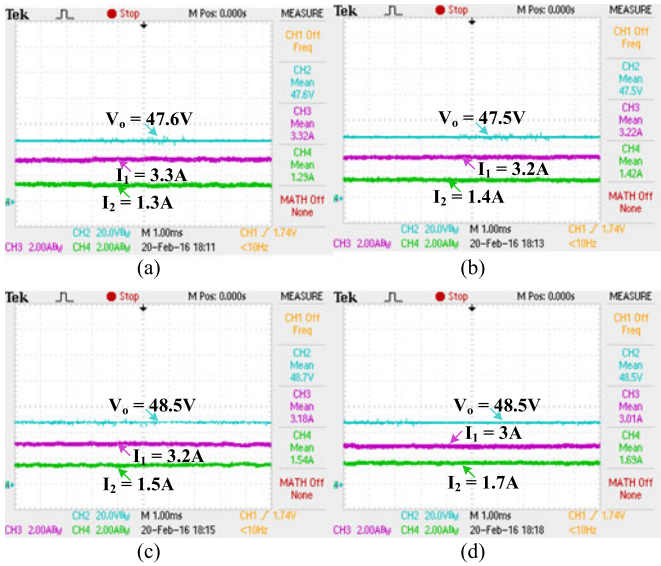

Fig. 16. Converter output currents (2 A/div) and dc-bus voltage (20 V/div) for a load of 220 W, with (a) HDG; (b) PDC; (c) PDCVC IP shift; and (d) PDCVC TB shift method.

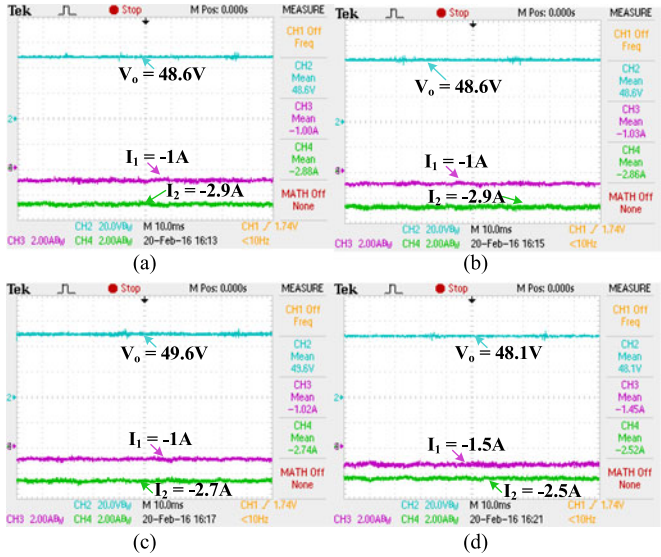

Fig. 17. Converter output currents (2 A/div) and dc-bus voltage (20 V/div) for a load of –200 W, with (a) HDG, (b) PDC, (c) PDCVC IP shift, and (d) PDCVC TB shift method.

the proposed method is validated experimentally under light and heavy load, and dynamic load changing conditions.

A. *Heavy-Loading Conditions*

Figs. 14 and 15 show the experimental results for the proposed droop control methods for a total load of $\pm$500 W. From Fig. 15, it can be seen that the current-sharing error is minimum for the PDCVC method with TB shift. However, its voltage regulation is slightly beyond the limit set by the design, which is 2.5%. Nevertheless, the dc-bus voltage for the PDCVC method with TB shift is within the boundaries specified by the standards. Also,

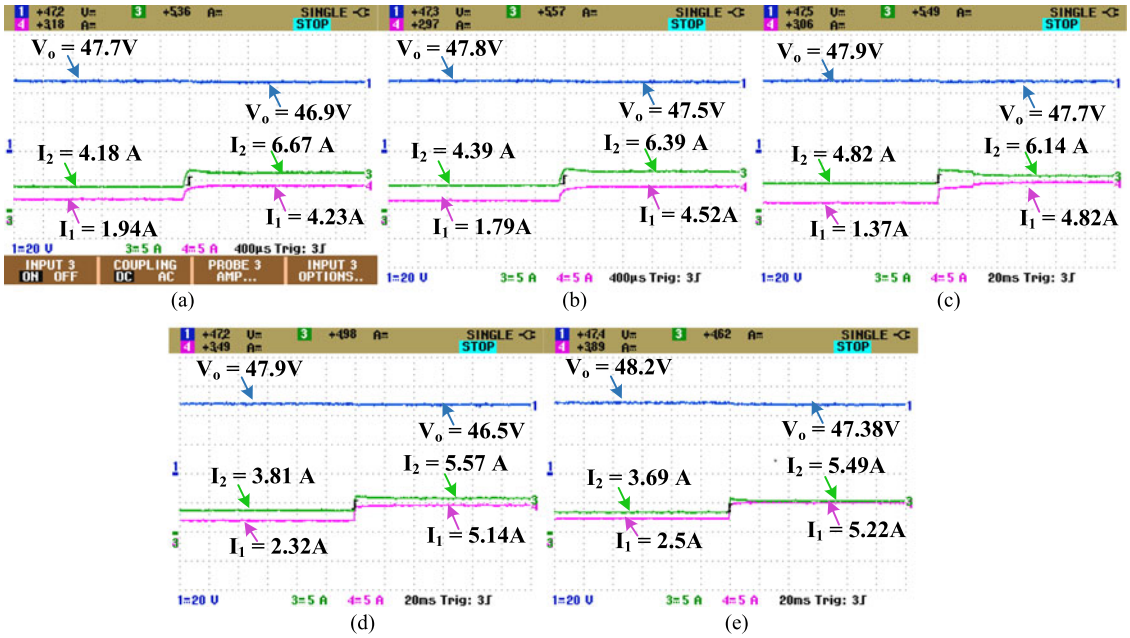

Fig. 18. Converter output currents (5 A/div) and dc-bus voltage (20 V/div) during step change in load from 300 W to 525 W, with (a) LD [14]; (b) IP droop [17]; (c) HDG; (d) PDC; and (e) PDCVC TB shift method.

the voltage regulation is within limits for the HDG method. As expected, the voltage regulation in case of the PDCVC method with IP shift is poor in the negative loading conditions (i.e., for −500 W) due to the reasons explained in Section III-B. Hence, the PDCVC method with IP shift is more suitable for applications where the converters will be predominantly be operating in positive loading conditions.

B. Light-Loading Conditions

Figs. 16 and 17 show the experimental results for a total load of 220 and –200 W, respectively. From Fig. 16, it can be observed that the voltage regulation is within limits for all the methods. Furthermore, for a total load of 220 W, it can be seen that the PDCVC method with TB shift offers the best current-sharing accuracy. From Fig. 17, it can be observed that the PDCVC method with TB shift offers the best current sharing and voltage regulation among all the methods.

C. Dynamic Loading Conditions (With Step Change in Load)

Fig. 18 shows the experimental results during a step change in load from 300 to 525 W. These results are obtained with cable resistance $R_1 = 50\ \text{m}\Omega$ and $R_2 = 20\ \text{m}\Omega$, voltage sensor errors of 1.5%, and current sensor error of 0.5%. It is observed that during step load change, all the proposed methods remain stable and the overshoots in the converter output currents also remain of the same order. However, the settling time for the HDG method is observed to be higher compared to the conventional droop control methods but this is expected as there is a shift from linear to nonlinear modes. In the case of PDC and PDCVC methods, the settling time is almost the same as the conventional methods. Nevertheless, the main objective of the proposed work was to achieve a better tradeoff between current sharing and voltage

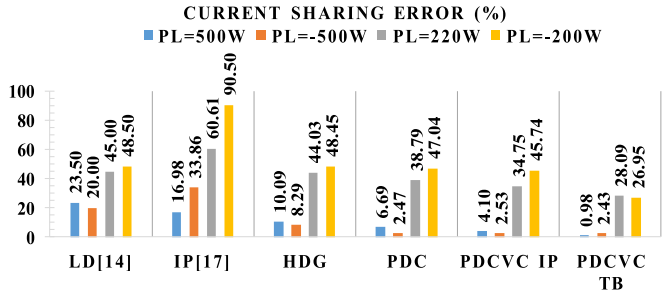

Fig. 19. Current-sharing performance comparison of the proposed methods.

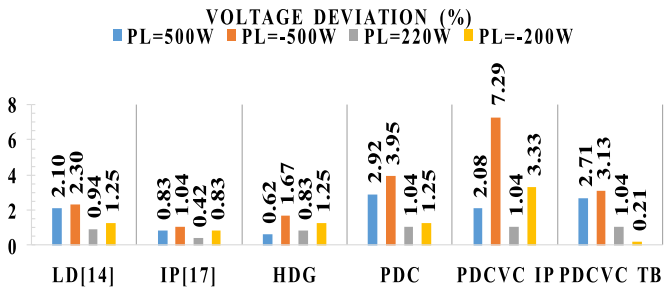

Fig. 20. Voltage regulation performance comparison of the proposed methods.

regulation at steady state. This is achieved using the proposed schemes, and it remains unaltered even during step change in the load.

VI. Conclusion

Proportional load sharing (as per the power rating) and good voltage regulation are desired in a dc microgrid operation. Otherwise, there would be large circulating currents, thermal stress on the power-electronic converters, and poor power

quality in the dc microgrid. In this paper, the issues of load sharing and voltage regulation in a dc microgrid environment were analyzed and presented. The effects of cable resistance and sensing/calibration errors on the dc microgrid performance were investigated. Three novel nonlinear droop control schemes were proposed, analyzed, and implemented to improve the current-sharing accuracy, and, hence, the overall reliability of the system. It was observed that the proposed techniques significantly enhance the current-sharing accuracy for a given voltage deviation. The performance comparison of the proposed techniques was carried out and analyzed. These results are consolidated and presented in Figs. 19 and 20.

From Section III-A and Figs. 14 to 19, it can be concluded that the HDG method offers the best voltage regulation among all the proposed methods. However, its current-sharing accuracy is not as good as the other two techniques at high-load conditions. Furthermore, under light loads, its current-sharing accuracy is almost the same as the conventional linear droop method. Hence, the HDG method is suitable for applications that demand stiff voltage regulation under all load conditions and considerable current-sharing accuracy at low- and high-loading conditions. It is also seen that the PDC method offers good load sharing and considerable voltage regulation under all loading conditions. However, it does not provide stiff voltage regulation under heavy-loading conditions. Hence, the PDC method can be utilized where rigid voltage regulation is not mandatory. Fig. 19 shows that the PDCVC method with TB shift offers the best current sharing among all the methods. Furthermore, the voltage regulation for this method is within the acceptable range as specified by the standards (i.e., $\leq 5\%$). Also, it can be seen that for the same voltage regulation, the current-sharing performance is better than the conventional methods. Hence, the PDCVC method with TB shift is suitable for applications that demand stiff current-sharing accuracy under all loading conditions except in the vicinity of no load (i.e., for $|Ii| \leq 0.1$ p.u.), where the current-sharing performance is poor. It can also be concluded that the PDCVC method with IP shift is more favourable when the converters are operated predominantly under positive loading conditions.

In summary, it can be concluded that the tradeoff between the current sharing and voltage regulation is better in the proposed methods compared to the conventional methods.

APPENDIX

This section presents the derivation of the state matrices for the proposed droop control methods. The derived state matrices are further used in the stability analysis. By applying KVL in the circuit of Fig. 9, the following set of equations is obtained:

$$\frac{di_1}{dt} = i_1' = -\frac{1}{L_1}v_b + \frac{1}{L_1}v_1 - \frac{R_1}{L_1}i_1\,;$$
$$i_2' = -\frac{1}{L_2}v_b + \frac{1}{L_2}v_2 - \frac{R_2}{L_2}i_2\,. \tag{A1}$$

By applying KCL at node A [see Fig. 9], the following equation is obtained:

$$i_L' = i_1' + i_2' = \frac{v'_b}{R_{eqL}},\ \text{where}\ R_{eqL} = \left(\frac{R_{\text{CPL}} \times R_{\text{CIL}}}{R_{\text{CPL}} + R_{\text{CIL}}}\right). \tag{A2}$$

Substituting (A1) into (A2), leads to the following equation:

$$v_b' = -\left(\frac{R_{eqL}}{L_1} + \frac{R_{eqL}}{L_2}\right)v_b + \frac{R_{eqL}}{L_1}v_1 + \frac{R_{eqL}}{L_2}v_2 - \frac{R_{eqL}R_1}{L_1}i_1 - \frac{R_{eqL}R_2}{L_2}i_2. \tag{A3}$$

The plant transfer function for the boost converter with the specifications given in Tables II and III is obtained as follows:

$$G_v = \frac{\hat{v}_0}{\hat{d}} = \frac{-1.757 \times s^2 - 1.144 \times 10^4 \times s + 2.865 \times 10^7}{s^2 + 593.9 \times s + 3.056 \times 10^5}. \tag{A4}$$

Using the k-factor approach, a type-III voltage compensator is designed and is given as follows:

$$T_v = \frac{1.325 \times 10^4 s^2 + 4.454 \times 10^6 \times s + 5.613 \times 10^8}{s^3 + 3.452 \times 10^4 \times s^2 + 2.98 \times 10^8 \times s}. \tag{A5}$$

From (A4), (A5), and Fig. 8, the closed-loop transfer function is obtained as follows:

$$\frac{V_i}{V_i^{\text{ref}}} = \frac{G_v \times T_v}{1 + G_v \times T_v} = \frac{num(s)}{den(s)}. \tag{A6}$$

The transfer function in (A6) is simplified using appropriate approximations such that the converter dynamics are preserved. The simplified plant transfer function is given as follows:

$$\frac{V_i}{V_i^{\text{ref}}} = \frac{1}{\tau s + 1} = \frac{1}{(1/5794)s + 1}. \tag{A7}$$

From (8) and (A7), the following equations can be derived:

$$v_1' = -\frac{1}{\tau}v_1 - \frac{nk_1 i_1^{n-1}}{\tau}i_1\,;\quad v_1' = -\frac{1}{\tau}v_2 - \frac{nk_2 i_2^{n-1}}{\tau}i_2\,. \tag{A8}$$

From (23)–(25), (A1)–(A3), (A8), the state matrix for the HDG method (A_{HDG}) is computed and is given as follows:

$$A_{\text{HDG}} = \begin{bmatrix} -R_{eqL}\left(\frac{1}{L_1}+\frac{1}{L_2}\right) & \frac{R_{eqL}}{L_1} & \frac{R_{eqL}}{L_2} & -\frac{R_{eqL}R_1}{L_1} & -\frac{R_{eqL}R_2}{L_2} \\ 0 & -\frac{1}{\tau} & 0 & -\frac{nk_1 I_1^{n-1}}{\tau} & 0 \\ 0 & 0 & -\frac{1}{\tau} & 0 & -\frac{nk_2 I_2^{n-1}}{\tau} \\ -\frac{1}{L_1} & \frac{1}{L_1} & 0 & -\frac{R_1}{L_1} & 0 \\ -\frac{1}{L_2} & 0 & \frac{1}{L_2} & 0 & -\frac{R_2}{L_2} \end{bmatrix}. \tag{A9}$$

In a similar manner, the state matrices for PDC and PDCVC methods can be derived.

REFERENCES

[1] F. Blaabjerg, Z. Chen, and S. B. Kjaer, "Power electronics as efficient interface in dispersed power generation systems," *IEEE Trans. Power Electron.*, vol. 19, no. 5, pp. 1184–1194, Sep. 2004.

[2] V. Nasirian, S. Moayedi, A. Davoudi, and F. L. Lewis, "Distributed cooperative control of DC microgrids," *IEEE Trans. Power Electron.*, vol. 30, no. 4, pp. 2288–2303, Apr. 2015.

[3] H. Kakigano, Y. Miura, and T. Ise, "Low-voltage bipolar-type DC microgrid for super high quality distribution," *IEEE Trans. Power Electron.*, vol. 25, no. 12, pp. 3066–3075, Dec. 2010.

[4] Y. Gu, W. Li, and X. He, "Frequency-coordinating virtual impedance for autonomous power management of DC microgrid," *IEEE Trans. Power Electron.*, vol. 30, no. 4, pp. 2328–2337, Apr. 2015.

[5] Y. K. Chen, Y. C. Wu, C. C. Song, and Y. S. Chen, "Design and implementation of energy management system with fuzzy control for DC microgrid systems," *IEEE Trans. Power Electron.*, vol. 28, no. 4, pp. 1563–1570, Apr. 2013.

[6] P. Klimczak and S. Munk-Nielsen, "Comparative study on paralleled vs. scaled dc-dc converters in high voltage gain applications," in *Proc. 13th Int. Power Electron. Motion Contr. Conf.*, Poland, Sep. 2008, pp. 108–113.

[7] Y. Huang and C. K. Tse, "Circuit theoretic classification of parallel connected DC–DC converters," *IEEE Trans. Circuits Syst. I, Reg. Papers*, vol. 54, no. 5, pp. 1099–1108, May 2007.

[8] S. Anand, B. G. Fernandes, and J. Guerrero, "Distributed control to ensure proportional load sharing and improve voltage regulation in low-voltage dc microgrids," *IEEE Trans. Power Electron.*, vol. 28, no. 4, pp. 1900–1913, Apr. 2013.

[9] P. H. Huang, P. C. Liu, W. Xiao, and M. S. El Moursi, "A novel droop-based average voltage sharing control strategy for DC microgrids," *IEEE Trans. Smart Grid*, vol. 6, no. 3, pp. 1096–1106, May 2015.

[10] P. Wang, X. Lu, X. Yang, W. Wang, and D. Xu, "An improved distributed secondary control method for dc microgrids with enhanced dynamic current sharing performance," *IEEE Trans. Power Electron.*, vol. 31, no. 9, pp. 6658–6673, Sep. 2016.

[11] X. Lu, J. M. Guerrero, K. Sun, and J. C. Vasquez, "An improved droop control method for dc microgrids based on low bandwidth communication with dc bus voltage restoration and enhanced current sharing accuracy," *IEEE Trans. Power Electron.*, vol. 29, no. 4, pp. 1800–1812, Apr. 2014.

[12] B. Wang, M. Sechilariu, and F. Locment, "Intelligent DC microgrid with smart grid communications: Control strategy consideration and design," *IEEE Trans. Smart Grid*, vol. 3, no. 4, pp. 2148–2156, Dec. 2012.

[13] J. Rajagopalan, K. Xing, Y. Guo, F. C. Lee, and B. Manners, "Modeling and dynamic analysis of paralleled dc/dc converters with master-slave current sharing control," in *Proc. IEEE Appl. Power Electron. Conf. Expo.*, Mar. 1996, vol. 2, pp. 678–684.

[14] B. T. Irving and M. M. Jovanovic, "Analysis, design, and performance evaluation of droop current-sharing method," in *Proc. IEEE Appl. Power Electron. Conf.*, New Orleans, LA, USA, Feb. 2000, vol. 1, pp. 235–241.

[15] Y. Ito, Y. Zhongqing, and H. Akagi, "DC microgrid based distribution power generation system," in *Proc. IEEE Int. Power Electron. Motion Contr. Conf.*, China, Aug. 2004, vol. 3, pp. 1740–1745.

[16] J. W. Kim, H. S. Choi, and B. H. Cho, "A novel droop method for converter parallel operation," *IEEE Trans. Power Electron.*, vol. 17, no. 1, pp. 25–32, Jan. 2002.

[17] F. Chen, R. Burgos, D. Boroyevich, and W. Zhang, "A nonlinear droop method to improve voltage regulation and load sharing in dc systems," in *Proc. Int. Conf. DC Microgrids*, Atlanta, GA, USA, Jun. 2015, pp. 45–50.

[18] A. Khorsandi, M. Ashourloo, and H. Mokhtari, "A decentralized control method for a low-voltage DC microgrid," *IEEE Trans. Energy Convers.*, vol. 29, no. 4, pp. 793–801, Dec. 2014.

[19] C. Wei, Y. Daopei, C. Jialin, W. Yongzhi, and Y. Yuxing, "The impact of line resistance on load sharing and an improved droop control of dc microgrid," in *Proc. 9th Int. Conf. Power Electron. ECCE Asia*, South Korea, Jun. 2015, pp. 208–212.

[20] Y. Goyal, "Droop control techniques to enhance voltage regulation and load sharing accuracy in dc microgrid," M.S. thesis, Dept. Electr. Eng., , Indian Inst. Technol.Bombay, Mumbai, India, 2016.

[21] I. U. Nutkani, W. Peng, P. C. Loh, and F. Blaabjerg, "Autonomous economic operation of grid connected dc microgrid," in *Proc. IEEE 5th Int. Symp. Power Electron. Distrib. Gener. Syst.*, Ireland, Jun. 2014, pp. 1–5.

[22] P. Lancaster and K. Salkauskas, *Curve and Surface Fitting: An Introduction*, vol. 4. San Diego, CA, USA: Academic, 1986.

[23] F. Gao, S. Bozhko, G. Asher, P. Wheeler, and C. Patel, "An improved voltage compensation approach in a droop-controlled dc power system for the more electric aircraft," *IEEE Trans. Power Electron.*, vol. 31, no. 10, pp. 7369–7383, Oct. 2016.

[24] A. M. Rahimi and A. Emadi, "An analytical investigation of DC/DC power electronic converters with constant power loads in vehicular power systems," *IEEE Trans. Veh. Technol.*, vol. 58, no. 6, pp. 2689–2702, Jul. 2009.

[25] M. Wu and D. D. C. Lu, "A novel stabilization method of LC input filter with constant power loads without load performance compromise in DC microgrids," *IEEE Trans. Ind. Electron.*, vol. 62, no. 7, pp. 4552–4562, Jul. 2015.

[26] R. W. Erickson and D. Maksimovic, *Fundamentals of Power Electronics*. New York, NY, USA: Kluwer, 2001.

[27] H. D. Venable, "The k-factor: A new mathematical tool for stability analysis and synthesis," in *Proc. Powercon 10 Conf.*, San Diego, CA, USA, Mar. 1983.

Prajof Prabhakaran (S'16) received the B.Tech. degree in electrical and electronics engineering (EEE) and the M.Tech. degree in power electronics from Amrita Vishwa Vidyapeetham, Coimbatore, India, in 2009 and 2011, respectively. He is currently working toward the Ph.D. degree in power electronics and power systems from the Department of Electrical Engineering, Indian Institute of Technology Bombay, Mumbai, India.

From July 2011 to June 2013, he was an Assistant Professor in the EEE Department, Amrita School of Engineering, Coimbatore. His research interests include dc microgrids, ac/dc grid-tied renewable energy systems, and dc–dc power converters.

Yogendra Goyal received the B.Tech. degree in electrical engineering from Indian Institute of Technology (IIT) Jodhpur, India, in 2014, and the M.Tech. degree in power electronics from IIT Bombay, Mumbai, India, in 2016.

His research interests include dc microgrid, power-electronic converters, and renewable energy systems.

Vivek Agarwal, photograph and biography not available at the time of publication.